Crystal and magnetic structure of the oxypnictide superconductor $LaFeAsO_{1-x}F_x$: A neutron-diffraction study

N. Qureshi,[1,*] Y. Drees,[1] J. Werner,[2] S. Wurmehl,[2] C. Hess,[2] R. Klingeler,[2] B. Büchner,[2] M. T. Fernández-Díaz,[3] and M. Braden[1,†]

[1]*II. Physikalisches Institut, Universität zu Köln, Zülpicher Strasse 77, D-50937 Köln, Germany*

[2]*Leibniz-Institut für Festkörper- und Werkstoffforschung (IFW) Dresden, D-01171 Dresden, Germany*

[3]*Institut Max von Laue-Paul Langevin, 6 rue Jules Horowitz, BP 156, 38042 Grenoble Cedex 9, France*

(Received 23 February 2010; revised manuscript received 19 August 2010; published 11 November 2010)

High-resolution and high-flux neutron as well as x-ray powder-diffraction experiments were performed on the oxypnictide series $LaO_{1-x}F_xFeAs$ with $0 \leq x \leq 0.15$ in order to study the crystal and magnetic structure. The magnetic symmetry of the undoped compound corresponds to those reported for *RE*OFeAs (with *RE* a rare earth) and for AFe_2As_2(A=Ba, Sr) materials. We find an ordered magnetic moment of 0.63(1) μ_B at 2 K in LaOFeAs, which is significantly larger than the values previously reported for this compound. A sizable ordered magnetic moment is observed up to a F doping of 4.5% whereas there is no magnetic order for a sample with a F concentration of x=0.06. In the undoped sample, several interatomic distances and $FeAs_4$ tetrahedra angles exhibit pronounced anomalies connected with the broad structural transition and with the onset of magnetism supporting the idea of strong magnetoelastic coupling in this material.

DOI: 10.1103/PhysRevB.82.184521 PACS number(s): 61.50.Ks, 74.70.Xa, 75.30.Fv

I. INTRODUCTION

The recently discovered family of oxypnictides superconductors[1] has focused the interest of the scientific community as they represent the first noncopper-oxide-based layered superconductors reaching a T_c of 55 K.[2] Their crystal structure is similar to the one adopted by the copper-based superconductors, i.e., a layered structure where FeAs sheets are sandwiched by LaO/F sheets [Fig. 1(a)].

Like for the cuprates superconductivity arises by chemical doping and suppression of the magnetic ground state; however, also the application of pressure to the nondoped system can induce superconductivity for certain FeAs compounds[3–7] in clear contrast to the cuprates where the antiferromagnetic state of the parent phase is a Mott-Hubbard insulator requiring electronic doping in order to obtain metallicity and superconductivity. For $SmO_{1-x}F_xFeAs$ the magnetic ordered state even extends to doping levels within the superconducting regime and low-energy spin fluctuations have been observed up to the doping levels where T_c is maximal.[8] These findings suggest an important role of magnetism in the superconducting pairing.

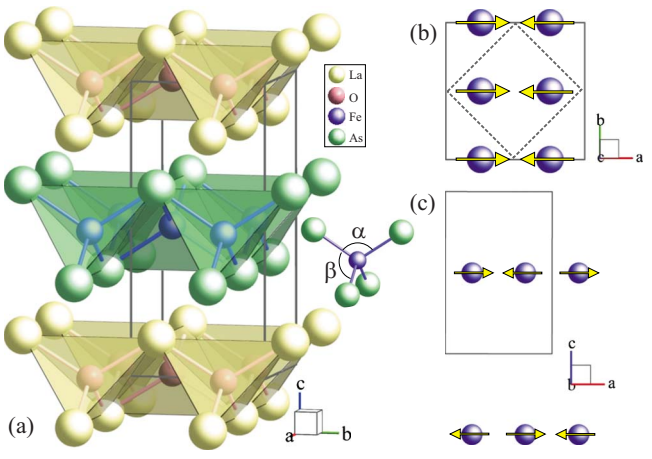

FIG. 1. (Color online) (a) Visualization of the tetragonal crystal structure of $LaO_{1-x}F_xFeAs$ and the definition of the As-Fe-As bond angles. (b) The magnetic structure only showing the Fe ions in the orthorhombic unit cell (straight line). The dashed line depicts the tetragonal cell. (c) Alternation of the moment direction along the c axis due to the propagation vector $\mathbf{k}=(1\ 0\ \frac{1}{2})$

The magnetism in the FeAs compounds appears to be very sensitive to the structural details which in turn modify the Fermi nesting conditions and the geometric frustration. It has even been stated that the structural distortions play a more important role in the modification of the Fermi surface than charge doping for inducing superconductivity.[9] The shape of the $FeAs_4$ tetrahedra seems to be decisive, as the highest superconducting transition temperatures are obtained for regular $FeAs_4$ tetrahedra.[10,11] This observation is corroborated by density-functional theory (DFT) calculations which reveal a clear dependence of the Fe magnetic moments as well as of the magnetic interaction parameters on the shape of the $FeAs_4$ layers, i.e., the FeAs bond distance and the layer thickness.[12]

In spite of serious experimental efforts there are still open issues concerning the magnetic and crystal structure of the $LaO_{1-x}F_xFeAs$ series. In particular, the reported low magnetic moment of only 0.36 μ_B per Fe in pure LaOFeAs (Ref. 13) is highly debated, as DFT calculations yield a far larger moment.[14] In first view, one could explain the reduced experimental moment through the suppression by magnetic fluctuations. But the DFT calculations more reliably predict that there is very little variation in the moment in the *RE*OFeAs series with different *RE*'s in striking contradiction to the report that the moment in LaOFeAs is much smaller than those in the other members of the series. In Ref. 15 the magnetic moment of the Fe was not determined by neutron diffraction but by the Mössbauer technique, therefore the absolute value suffers from the necessary assumptions. Note that the Mössbauer results, however, perfectly agree with the

DFT calculations in the fact that the moment of Fe varies only very little (less than 15%) in the *RE*OFeAs series.[16] There is thus an important inconsistency between the low Fe moment reported by neutron diffraction in LaOFeAs on the one hand and the DFT and the Mössbauer results on the *RE*OFeAs series on the other hand. Our distinct neutron-diffraction experiments yield a much larger ordered moment in LaOFeAs lifting this discrepancy to a large extent.

Several previous studies of lattice parameters, thermal expansion, resistivity, specific heat, and many other properties indicate anomalous behavior above and around the structural phase transition whose microscopic origin, however, remains unclear. Our detailed structure determinations as function of temperature allow us to identify all this anomalous behavior with strong magnetoelastic coupling, as we may identify the underlying behavior of the structural parameters. There are clear anomalies in the evolution of the FeAs bond lengths and of the tetrahedral angles, which are the parameters closely coupled to the size of the magnetic moment.

We have combined high-flux and high-resolution neutron and x-ray powder-diffraction experiments to study the magnetic and crystal structure of the $LaO_{1-x}F_xFeAs$ series. We may unambiguously determine the magnetic symmetry of the undoped material finding a sizeable ordered moment. The doping dependence of structural parameters qualitatively confirms earlier studies, but upon cooling through the structural and magnetic transitions, the pure and slightly doped materials exhibit anomalies in bond distances and in bond angles which reflect the general magnetophonon coupling in FeAs compounds.

II. EXPERIMENTAL

Powder samples of $LaO_{1-x}F_xFeAs$ have been synthesized using a previously reported two-step solid-state reaction method.[1,17,18] We mention that for our sample with the nominal F content $x=0.04$ investigated in this work, wavelength-dispersive x-ray analysis yields a higher F content as compared to a sample with the same nominal concentration which has been investigated in previous studies of our group, see, for example.[17,19,20] We therefore refer to the former sample by using the measured F content ($x=0.045$) in order to discriminate it from the latter and otherwise use the nominal doping levels throughout the paper.

Moreover, we note that for our sample with $x=0$, resistivity measurements suggest[17,21] $T_S \sim 152$ K [peak of $\rho(T)$] and $T_N \sim 135$ K [inflection point of $\rho(T)$], i.e., at somewhat lower temperatures as have been found in our previous undoped sample.[17,19–21]

The nuclear structure investigation of all powder samples ($0 \leq x \leq 0.15$) at room temperature (RT), 200, 100, and 2 K has been carried out at the high-resolution neutron powder diffractometer D2B (Institut Laue-Langevin, Grenoble), where the $x=0$ and 0.045 samples have been examined at additional temperatures. The experiments have been performed using the wavelength of 1.594 Å from the Ge(335) reflection. Powder-diffraction patterns have been recorded with a counting time of 3 h per temperature point. The magnetic structures of the samples with $0 \leq x \leq 0.06$ have been investigated at the high-flux neutron powder diffractometer D20 (ILL). A wavelength of 2.41 Å emerging from the (002) reflection of a pyrolytic graphite monochromator has been used, which gives a good compromise between high flux and reciprocal space resolution. Diffraction patterns have been recorded for 2 h above the magnetic transition and at various temperatures within the magnetically ordered phase. The same samples have been used for further experiments at an x-ray powder diffractometer Siemens D5000. Each x-ray diffraction pattern has been measured for 5 h using Cu $K\alpha$ radiation.

III. RESULTS AND DISCUSSION

A. Magnetic structure in pure and slightly doped LaOFeAs

The magnetic structure of LaOFeAs has not been unambiguously determined so far. First evidence for a spin-density wave instability was obtained from kinks in the resistivity and in the magnetic susceptibility further supported by electronic-structure calculations.[22] The pioneer diffraction experiments by De la Cruz *et al.* showed that a structural phase transition occurs slightly above the magnetic transition. The structural and magnetic transition temperatures amount to $T_S=155$ K and $T_N=137$ K, respectively.[13] As justified in detail below and in agreement with the findings for *RE*OFeAs and AFe_2As_2 we will assume an orthorhombic and not a monoclinic low-temperature phase in the following. The orthorhombic a_o and b_o axes are rotated by 45° degrees with respect to the tetragonal axes a_{tet}. The proposed magnetic structure consists of ferromagnetic stripes of neighboring Fe moments running along an orthorhombic axis antiferromagnetically stacked along the perpendicular axis, see Fig. 1(c). In the model initially proposed in Ref. 13 the stacking vector q_{stack} is perpendicular to the magnetic moment m_{Fe} which amounts to 0.36(5) μ_B at $T=8$ K. A following neutron diffraction and Mössbauer study on LaOFeAs by McGuire *et al.*[15] also reports a moment of 0.35 μ_B (determined by Mössbauer) but does not discuss the spin orientation. Huang *et al.*[23] describe a magnetic structure with q_{stack} parallel to the magnetic moment m_{Fe}, which disagrees with the earlier report,[13] but apparently the instrument resolution is insufficient to determine the spin direction along a_o or b_o.

We have analyzed all powder-diffraction patterns using the FULLPROF program.[24] The structural investigation at the high-resolution diffractometer D2B confirmed the correct phase formation of the tetragonal $P4/nmm$ and orthorhombic *Cmme* structures above and below the structural phase transition, respectively, see below. Figure 2 shows the high-resolution (D2B) and high-flux diffraction (D20) patterns of the $x=0.02$ sample at $T=2$ K.

In order to focus on the weak magnetic scattering the D20 diffraction patterns of the paramagnetic phases have been subtracted from the respective patterns of the magnetically ordered phases. Note that throughout this paper all D20 patterns are shown with exactly the same scale factor as normalized by the monitor. For the undoped sample the differences are manifest in two well-defined magnetic peaks, indexed as $(10\frac{1}{2})$ and $(10\frac{3}{2})$ at $2\theta=25.8°$ and 34.6°, respectively, to which a magnetic structure model has been refined

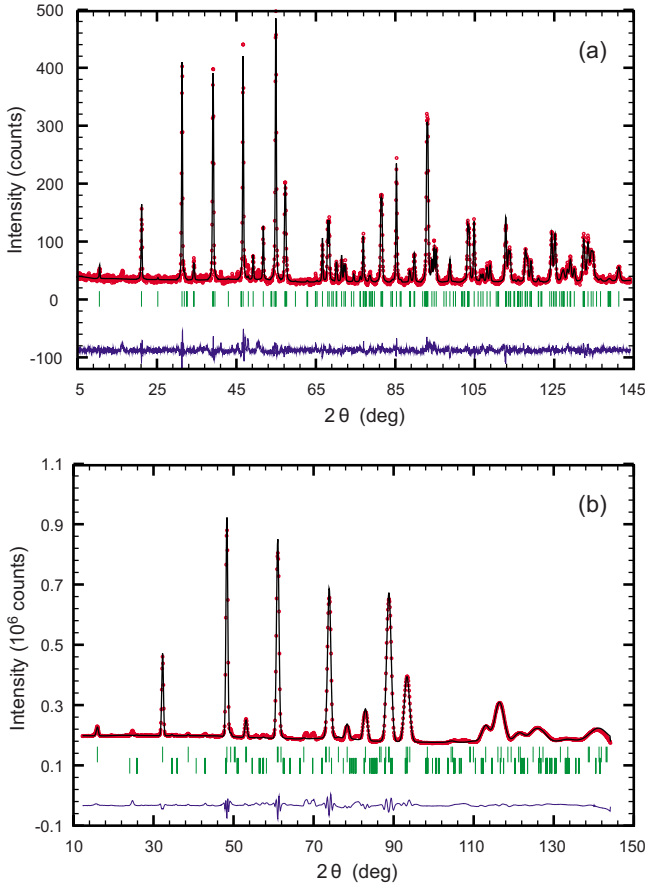

FIG. 2. (Color online) Diffraction patterns recorded with the $x=0.02$ sample at a temperature of $T=2$ K (a) at the high-resolution powder diffractometer D2B ($\lambda=1.594$ Å) and (b) at the high-flux powder diffractometer D20 ($\lambda=2.41$ Å). Dots represent the observed patterns while the respective upper (lower) lines show the calculated patterns (difference plots). The (green) markers indicate the positions of nuclear and magnetic [second row of markers in (b)] Bragg reflections.

(Fig. 3). Representation analysis[25,26] has been used to derive those magnetic structure models which are compatible with the nuclear structure (*Cmme*) and with the propagation vector with a half-indexed c^* component and an antiferromagnetic coupling between two Fe moments related by the C centering: $(1\ 0\ \frac{1}{2})$.[27] Out of the six possible collinear spin configurations [three directions along the principal crystallographic axes and the coupling between the two moments chosen at (0.25,0.0,0.5) and (0.75,0.0,0.5) in orthorhombic notation] only two may describe the data sufficiently well. These are the models with q_{stack} parallel to the magnetic moment m_{Fe}. Since neutron diffraction only measures the magnetic component perpendicular to the scattering vector, the models with q_{stack} perpendicular to the magnetic moment m_{Fe} proposed in Ref. 13, can be clearly excluded. To decide between the alignment of the magnetic moments along a_o or b_o is more difficult but due to the high statistics and resolution of the D20 data this is possible as well.

The solid (black) and dashed lines in Fig. 3 show the calculated patterns corresponding to the models where the moments are aligned along the a_o axis and along the b_o axis,

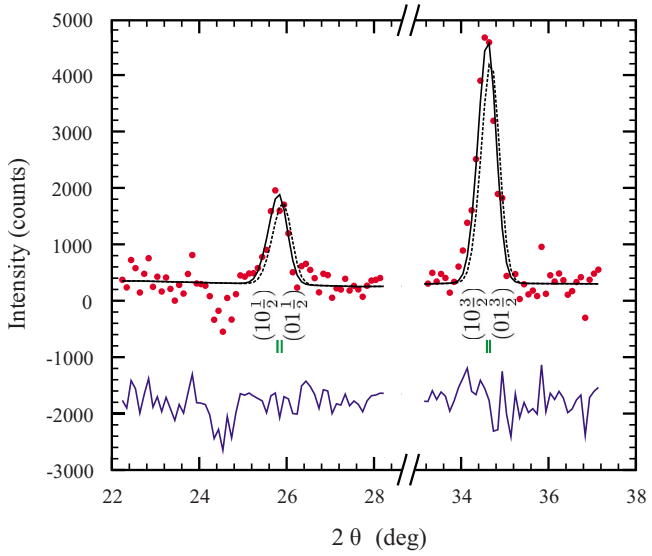

FIG. 3. (Color online) Extract of the observed pattern (dots), calculated patterns (upper lines), and difference plot (lower line) of two magnetic models for LaOFeAs. The calculated patterns result from magnetic structure models with the Fe magnetic moments along the *a* axis (straight line) and along the *b* axis (dashed line).

respectively. As the b_o axis is 0.4% shorter compared to a_o the two models can be distinguished. The model with the magnetic moments along the *a* axis is better suited to describe the observed peaks which is also expressed by the respective *R* values (10.71% for $\mu \| a$ and 12.76% for $\mu \| b$). The Fe magnetic moment along the *a* axis has been refined to 0.63(1) μ_{B} which is about twice the size of the magnetic moment presented in Refs. 13 and 15. Regarding this substantial difference great care has been taken concerning the reliability of the presented result. Therefore, three different refining methods have been used. The first method consisted of using a nuclear phase and a purely magnetic phase both being orthorhombic and having the same scale factor. The magnetic phase has been described with the same unit cell as the nuclear one by using the propagation vector $\mathbf{k}=(10\frac{1}{2})$. The second method was to handle nuclear and magnetic scattering from one single phase. The third method is similar to the second but the magnetic unit cell has been doubled along the *c* axis which means that no propagation vector has been used. All of the above refinement methods yielded exactly the same result. Figure 4 shows an extract of the D20 diffraction pattern focusing on the magnetic $(10\frac{3}{2})$ reflection and the strong nuclear (002) reflection. The respective integrated intensities emerging from the refinement are given in the figure allowing for the reconstruction of the magnetic scaling. Note, that there is no indication for significant preferred orientation in our sample, as it can be safely extracted from the full Rietveld fits.

The ordered moment at the Fe site still seems to be substantially lower than in other undoped FeAs compounds[28] but the difference is much smaller than previously reported. In particular, the variation within the *RE*OFeAs series is reduced in better agreement with DFT calculations and with recent Mössbauer studies which find only 15% variation in the magnetic moment within the entire series.[16]

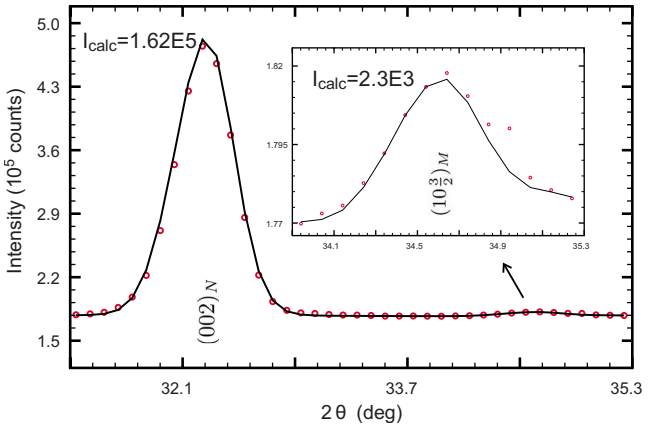

FIG. 4. (Color online) Extract of the observed (dots) and calculated D20 pattern (solid line). The inset magnifies the magnetic $(10\frac{3}{2})$ reflection. The respective integrated intensities are given in order to scale the magnetic scattering with respect to the nuclear one.

The same magnetic model was used to describe the data for the slightly doped samples. The refined magnetic moments for the $x=0.02$ and $x=0.045$ samples are 0.59(2) μ_B and 0.32(2) μ_B, respectively. For samples with $x \geq 0.06$ no magnetic scattering could be observed. The three powder samples revealing magnetic order have been investigated in more detail as a function of temperature. Figure 5 shows the temperature- and doping-dependent suppression of the magnetic order.

One can observe that the undoped and the $x=0.02$ sample exhibit similar magnetic moments with a similar temperature dependence but the magnetic reflections of the doped sample

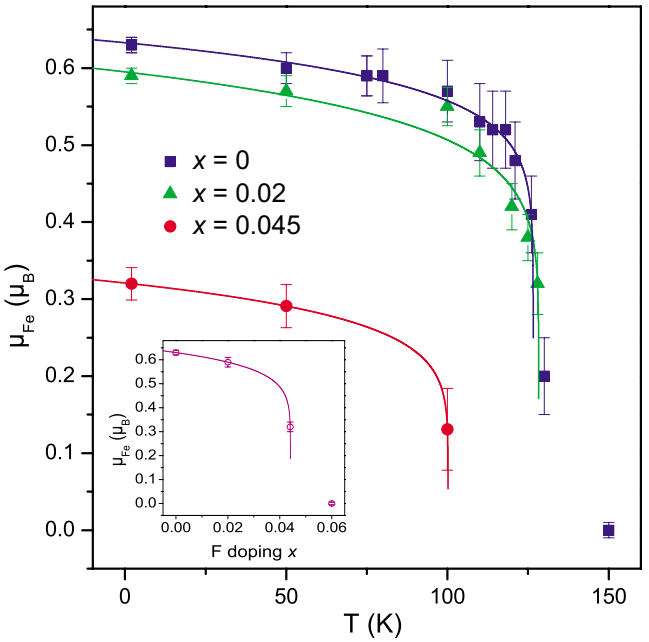

FIG. 5. (Color online) Magnetic moment of the Fe ions in dependence of temperature and F doping (inset, 2 K). Power-law functions have been fitted to the data as guide to the eyes (solid lines).

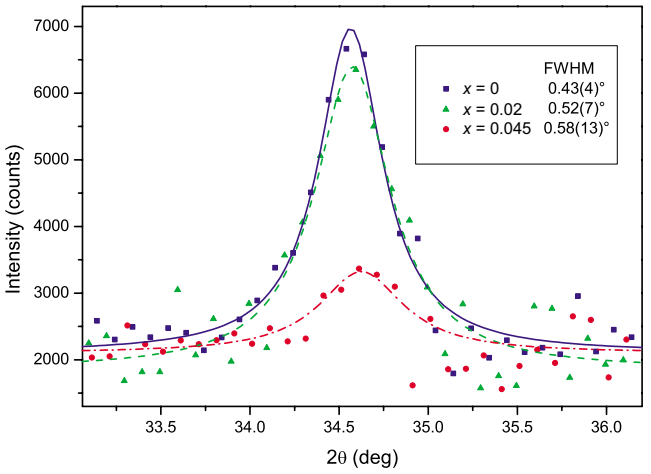

FIG. 6. (Color online) Data points show the magnetic $(10\frac{3}{2})$ reflection of the $x=0$, 0.02, and 0.045 samples. The FWHM have been extracted from pseudo-Voigt fits and reveal a broadening with increasing doping level.

exhibit a slightly broader full width at half maximum (FWHM) than those of the undoped sample (Fig. 6). A decrease in the coherence length would be in perfect agreement with the subsequent suppression of magnetic order, which is then expressed by the strongly reduced magnetic moment for $x=0.045$ and finally by the absence of long-range order for $x=0.06$. However, we may not fully rule out that the broadening of the magnetic peaks is due to an incommensurate magnetic order; but in case of the $x=0.02$ sample such an effect must be small.

B. Crystal structure in LaOFeAs

The crystal structure of LaOFeAs was studied by high-resolution neutron diffraction and by x-ray powder diffraction. The structural phase transition forms the most prominent feature in the temperature dependence of the crystal structure. In agreement with most previous studies we find that the low-temperature phase is orthorhombic, space group *Cmme*; the refinement of the structure model in the monoclinic space group proposed in Ref. 13 did not yield a better data description; the structural parameters given in Ref. 13 clearly worsen the reliability factors. However, the phase transition from $P4/nmm$ to *Cmme* seems to be quite uncommon. This transition is of the proper ferroelastic character and it can be directly related to the magnetism. The magnetic order at low temperature exhibits an orthorhombic symmetry due to the alignment and the stacking of the ferromagnetic stripes and due to the fixed orientation of the magnetic moments. Therefore, the crystal structure in the magnetic phase must become orthorhombic.[14] There is, however, another role of the orthorhombic distortion: it lifts the magnetic frustration. The magnetic structure is stabilized by a large next-nearest-neighbor Fe-Fe interaction [along the diagonals of the Fe square lattice, see Fig. 1(b)] but within the tetragonal symmetry the nearest-neighbor interactions are fully frustrated yielding two antiferromagnetic sublattices which are completely decoupled. Depending on the arbitrary choice of

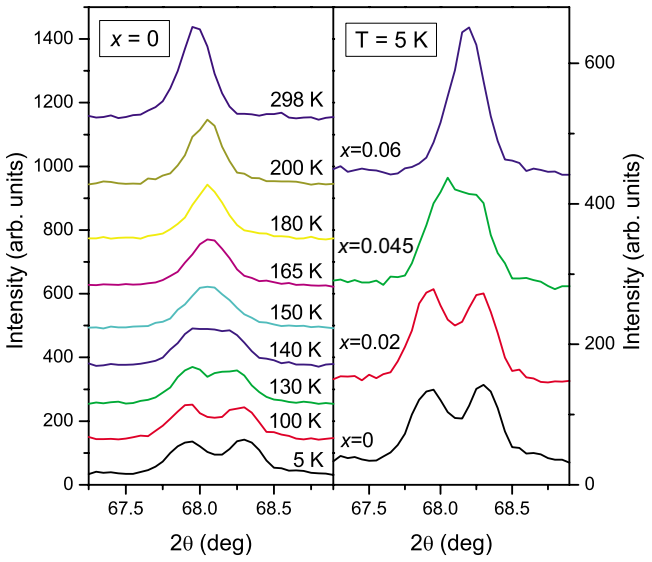

FIG. 7. (Color online) The structural phase transition is revealed by the temperature- (left panel) and doping-dependent (right panel) splitting of the tetragonal (220) reflection into the orthorhombic (400) and (040) reflections.

the coupling of the two subsystems, the ferromagnetic stripes run either along the *a* or along the *b* directions in orthorhombic notation. It is thus the role of the tetragonal-to-orthorhombic phase transition to lift the magnetic degeneracy and the frustration very similar to the magnetoelastic coupling recently studied in the vanadium oxyhalide VOCl.[29] The occurrence of magnetism in LaOFeAs can be considered as an electronic nematic phase but the magnetic in-plane anisotropy is only a natural consequence of the fact that the magnetic structure breaks the tetragonal rotation axis. The similarity with liquid-crystal phases is furthermore limited, as the high-temperature phase in LaOFeAs only exhibits a fourfold and not a continuous rotations symmetry. Nevertheless, one may associate the orthorhombic phase and its precursors with an electronic nematic state, and indeed resistivity measurements on detwinned $Ba(Fe/Co)_2As_2$ crystals reveal a pronounced electronic anisotropy.[30]

At low temperature the orthorhombic splitting in LaOFeAs is well documented, for example, by the neutron-diffraction profiles of the (400)/(040) reflections, see Fig. 7. Close to the structural transition these two reflections, however, overlap due to the smaller orthorhombicity in the neutron and in the x-ray experiments. The neutron data were used to refine the orthorhombic structure model up to 180 K and with the x-ray data we fitted the total width of the (400)/(040) scattering. Considering the steepest temperature dependencies of the orthorhombicity and of the peak width, one may determine the structural transition temperature to about $T_S \sim 150$ K, which perfectly coincides with the well-defined kink in the resistivity[17] and with the maximum in the thermal expansion coefficient,[20] both measured on nearly identical samples. However, the broadening of the (400)/(040) scattering as well as a finite orthorhombicity remain clearly visible above T_S, they only vanish at a temperature of about 200 K. These findings fully agree with similar diffraction studies by McGuire *et al.*[15] and by Nomura *et al.*[31] indicating that this feature is not sample specific but an intrinsic property of LaOFeAs. Great care is thus needed to determine the *true* structural phase transition temperature in $LaO_{1-x}F_xFeAs$ with the aid of diffraction data only. The broadening of the peaks in the intermediate temperature range should be interpreted as an inhomogeneous phase with strong local orthorhombic distortions as precursors of the long-range transition. The correlation length of the local orthorhombic distortions must be rather large, on the order of the coherence length of the radiation, i.e., of the order of several hundreds of angstroms. The broad temperature range, where orthorhombic precursors exist, seems to coincide with the upturn of the thermal-expansion coefficient well above the long-range structural transition[20] and with the upturn in the electric resistivity.[17] Evidence for orthorhombic precursors can also be deduced from the resistivity measurements on detwinned $Ba(Fe/Co)_2As_2$ crystals, as the anisotropy sets in already above the long-range structural transition.[30]

The high-resolution neutron data were used to refine structure models varying the cell constants, the *z* component of the La and As positions and the isotropic temperature factors of all species. From the refined parameters (see Table I) further structural aspects such as interatomic distances and angles have been deduced, see Fig. 9.

The temperature dependence of several structural aspects is shown in Figs. 9(c) and 9(d) for $x=0$ and $x=0.15$, respectively. The lattice constants show an expected dependence on temperature, but the remaining parameters reveal interesting features around the structural phase transition. In LaOFeAs, the interatomic distances and especially the tetrahedra angles reveal a strong discontinuity between 140 K and 180 K, which can be correlated with the onset of magnetic order (see Fig. 5) and to the occurrence of the orthorhombic precursors (see Fig. 8), respectively.

As this discontinuity might be a crucial result it has been assured that it is not a result of artifacts emerging from the refinement using the orthogonal unit cell instead of the tetragonal one. Therefore, all diffraction patterns have been analyzed as well with the microstrain option implemented in FULLPROF, which introduces an orthorhombic distortion into a tetragonal cell. The parameters obtained by this refinement method proved to be equivalent within the error bars. Additionally, a diffraction pattern from within the transition regime has been analyzed using two refined structural models of a tetragonal (just before the transition) and an orthogonal phase (just after the transition) by simply refining the respective scale factors. This procedure led to a considerably worse agreement implying that the broadening of the structural transition is a system-inherent property and not due to inhomogeneities in the chemical composition.

The orthorhombic precursors and the structural anomalies appear to be closely related with the electronic and magnetic properties. In the temperature range of the orthorhombic precursors the resistivity shows an upturn, whereas the long-range orthorhombic transition finally induces a decrease in resistivity, see, for example, Ref. 17. The magnetic importance of the structural transition is visible in the reduction in the magnetic susceptibility which can be interpreted by either a suppression of ferromagnetic fluctuations or an increase in the antiferromagnetic interaction. It appears inter-

TABLE I. Refined lattice constants, atomic parameters, and temperature factors of the $LaO_{1-x}F_xFeAs$ ($x=0$ and 0.15) nuclear structure investigation at selected temperatures. The respective Wyckoff sites are La $2c$ $\frac{1}{4}$ $\frac{1}{4}$ z, O/F $2a$ $\frac{3}{4}$ $\frac{1}{4}$ 0, Fe $2b$ $\frac{3}{4}$ $\frac{1}{4}$ $\frac{1}{2}$, As $2c$ $\frac{1}{4}$ $\frac{1}{4}$ z within the tetragonal space group $P4/nmm$ (origin choice 2) and La $4g$ 0 $\frac{1}{4}$ z, O/F $4a$ $\frac{1}{4}$ 0 0, Fe $4b$ $\frac{1}{4}$ 0 $\frac{1}{2}$, As $4g$ 0 $\frac{1}{4}$ z within the orthorhombic space group $Cmme$.

	2 K	100 K	150 K	165 K	180 K	200 K	RT
				$x=0$			
a (Å)	5.7063(4)	5.7057(4)	5.7000(4)	5.6974(2)	4.02758(4)	4.02814(4)	4.0322(2)
b (Å)	5.6788(4)	5.6799(4)	5.6890(4)	5.6920(2)	4.02748(4)	4.02814(4)	4.0322(2)
c (Å)	8.7094(6)	8.7113(6)	8.7151(6)	8.7167(1)	8.7191(1)	8.7218(1)	8.7364(4)
La z	0.1420(4)	0.1422(4)	0.1428(4)	0.1426(4)	0.1422(4)	0.1421(4)	0.1416(4)
As z	0.6505(5)	0.6503(5)	0.6491(6)	0.6493(6)	0.6502(6)	0.6504(5)	0.6508(5)
La B_{iso}	0.07(6)	0.17(6)	0.18(6)	0.24(6)	0.26(6)	0.25(6)	0.65(6)
As B_{iso}	0.12(7)	0.16(7)	0.26(8)	0.31(8)	0.27(8)	0.36(8)	0.62(8)
Fe B_{iso}	0.16(6)	0.19(6)	0.22(6)	0.29(6)	0.30(6)	0.36(6)	0.70(5)
O B_{iso}	0.20(8)	0.29(8)	0.34(8)	0.34(8)	0.33(8)	0.42(8)	0.84(8)
				$x=0.15$			
a (Å)	4.01739(3)	4.0182(2)				4.02065(3)	4.02447(3)
b (Å)	4.01739(3)	4.0182(2)				4.02065(3)	4.02447(3)
c (Å)	8.6610(1)	8.6651(4)				8.6769(1)	8.6948(1)
La z	0.1450(3)	0.1450(3)				0.1451(4)	0.1450(4)
As z	0.6536(4)	0.6534(4)				0.6540(4)	0.6540(4)
La B_{iso}	0.37(5)	0.36(5)				0.54(6)	0.73(5)
As B_{iso}	0.18(6)	0.26(6)				0.40(7)	0.58(6)
Fe B_{iso}	0.27(4)	0.27(4)				0.44(5)	0.66(4)
O/F B_{iso}	0.42(6)	0.35(6)				0.41(7)	0.73(7)

esting to note that the structural anomalies observed concern those structural parameters which are determining the size of the Fe moment, i.e., the FeAs distance and the FeAs layer thickness.[12] Furthermore, the structural anomalies indicate extrema in the temperature dependencies of the respective parameters, whereas a simple structural transition should induce a kink or a jump in the temperature dependency. These extrema, however, agree nicely with the anomalous contribution to the thermal expansion, which exhibits a sign change in the same temperature range and thus also yields an extremum for the anomalous component of the lattice volume.[20]

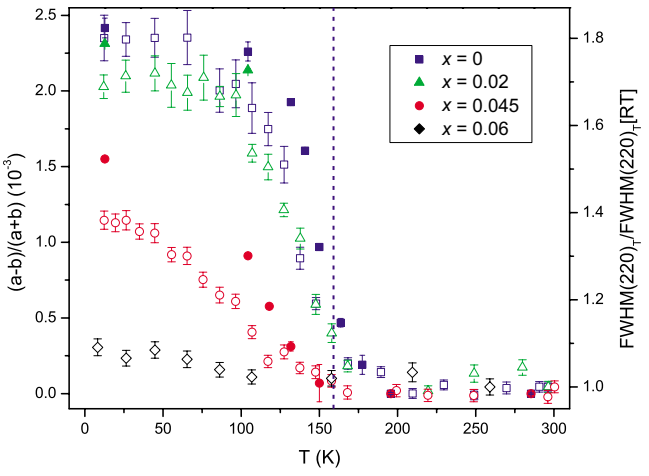

FIG. 8. (Color online) The tetragonal to orthorhombic phase transition expressed by the orthorhombicity $(a-b)/(a+b)$ (filled symbols, neutron diffraction) and the FWHM of the splitting $(220)_T$ reflection (open symbols, x-ray diffraction); the vertical dashed line indicates the structural transition temperature indicated by the resistivity and thermal-expansion anomalies in LaOFeAs.

C. Doping dependence of the crystal structure in $LaO_{1-x}F_xFeAs$

The tetragonal to orthorhombic transition has been studied by neutron diffraction in detail for two samples with $x=0$ and 0.045 and is represented in Fig. 8 by the orthorhombicity $(a-b)/(a+b)$. From the additional x-ray diffraction experiments, also including the $x=0.02$ and 0.06 samples, the temperature-dependent evolution of the FWHM of the splitting $(220)_T$ reflection has been extracted, where the obtained values have been normalized to the FWHM at RT.

It can be seen for $x \leq 0.045$ that the splitting of the a and b lattice constants in an orthorhombic fit, and therefore the broadening of the affected Bragg peaks, sets in well above the transition temperatures given in the literature.[15,19,31] No high-resolution neutron data has been collected for the $x=0.02$ sample between 100 and 200 K but the increase in the FWHM obtained by the x-ray experiments yields a broad transition regime very similar to the observation in the pure

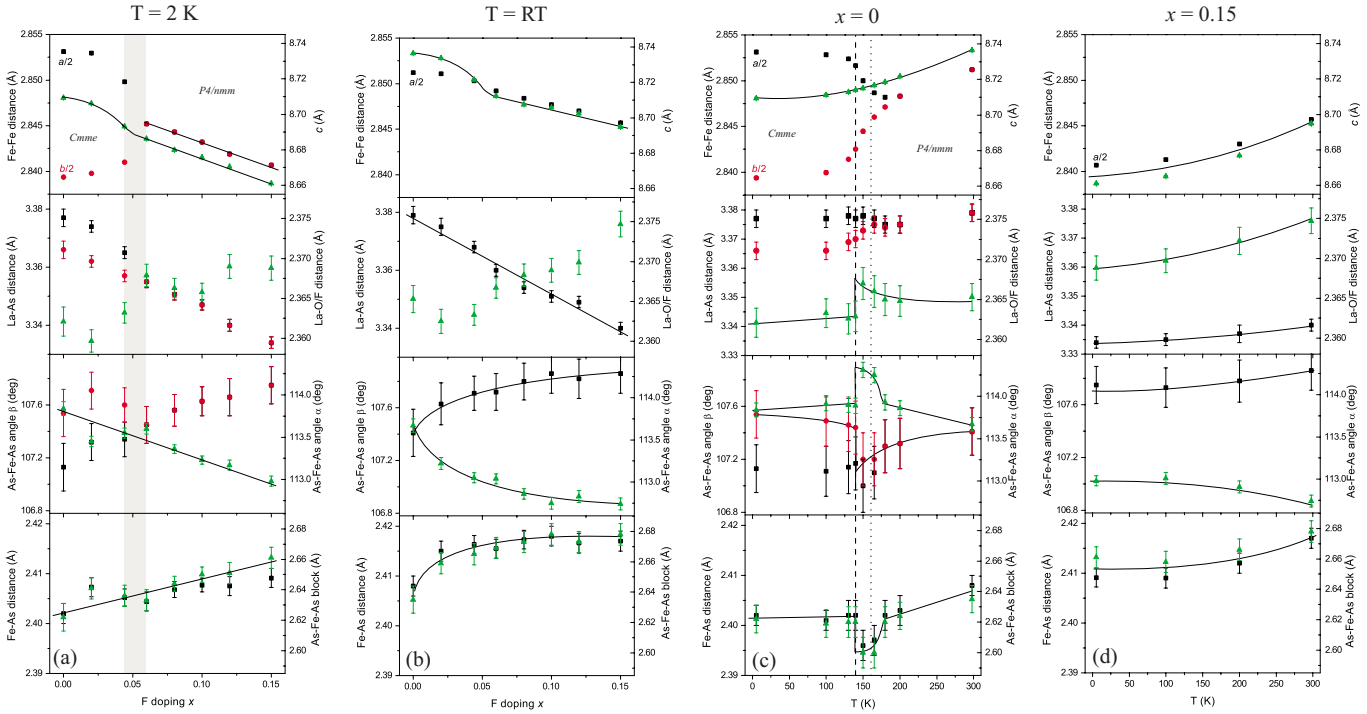

FIG. 9. (Color online) Structural parameters of the $LaO_{1-x}F_xFeAs$ compounds as a function of F doping [(a) $T=2$ K and (b) $T=$RT] and temperature [(c) $x=0$ and (d) $x=0.15$]. (Black) squares and (red) dots correspond to the left abscissa while (green) triangles belong to the right one. The gray shaded area in (a) denotes the doping-dependent structural phase transition regime. In (c) the dashed line marks the onset of static magnetism while the dotted line indicates the structural phase transition as taken from Ref. 17. Solid lines are guide to the eyes.

compound. The smearing of the structural phase transition by orthorhombic precursors is thus present over a finite doping interval. At the intermediate doping $x=0.045$, it is difficult to determine the structural transition temperature with the diffraction data, as the transition between the precursors and the long-range orthorhombic phase seems to be quite sluggish. The $x=0.06$ sample does not exhibit a comparable peak broadening indicating that the orthorhombic distortion is suppressed in the superconducting phase in $LaO_{1-x}F_xFeAs$. Note that also the previously studied superconducting sample with $x=0.05$ did not show the large peak broadening[19] in contrast with the nonsuperconducting $x=0.045$ sample studied here. In spite of the strong precursors associated with the structural transition, the long-range orthorhombic distortion seems to become very rapidly suppressed near $x=0.05$, i.e., at the boundary between superconducting and nonsuperconducting samples. However we may not fully rule out that some orthorhombic precursors persist into the superconducting phase.

The structural phase transition as a function of F doping is located at $0.045<x<0.06$, evidenced by the merging of the different Fe-Fe/La-As distances and As-Fe-As angles, which is shown in Fig. 9(a) for $T=2$ K. The doping-dependent evolution of the structural parameters does not exhibit any significant differences between $T=2$ K and RT [Fig. 9(b)], although the structural phase transition is only observed below 150 K. The lattice parameter c as well as the La-As distance decrease monotonically as a consequence of the charge carrier injection causing a Coulomb attraction of the LaO/F and FeAs layers. On the other hand the charge carrier injection into the FeAs layer leads to an increase in the Fe-As distance and of the As-Fe-As block thickness. The doping causes the $FeAs_4$ tetrahedra to become more homogeneous which is expressed by the different As-Fe-As angles approaching the perfect angle of 109.47°. Our findings are similar to those presented in Ref. 23 but extending to higher F concentrations.

The temperature dependence of the same structural aspects is shown in Fig. 9(d) for $x=0.15$. For this superconducting sample we find no structural anomaly in the temperature dependencies.

IV. CONCLUSIONS

We have performed high-resolution and high-flux neutron powder-diffraction experiments on the oxypnictide series $LaO_{1-x}F_xFeAs$, which on the one hand confirm the structural parameters and their evolution with F doping reported previously, but on the other hand our results indicate a structural anomaly and a larger magnetic order parameter.

With the high-resolution and good statistics of the diffraction data taken on the D20 diffractometer, we may unambiguously determine the magnetic structure in LaOFeAs obtaining a Fe magnetic moment of 0.63(1) μ_B which is in good agreement with a previous NMR study,[32] but about a factor two higher than previous neutron-diffraction, muon-spin-relaxation, and Mössbauer reports. The Fe magnetic moment has been subject of debate as it is largely reduced compared to the theoretically expected value of almost 2 μ_B.[12] Furthermore, the moment alignment is along the a axis parallel to the stacking direction of the ferromagnetic Fe stripes, which fully agrees with the magnetic structure ob-

served in other FeAs compounds. The 2% doped sample exhibits a similarly large magnetic moment, but from the magnetic reflection profile, i.e., from a broader FWHM, a perturbation of the static magnetic order can be deduced. We still find a sizeable ordered moment for a nonsuperconducting sample with $x=0.045$ in good agreement with muon-spin-relaxation and Mössbauer results.[19] Since this doping level is very close to the superconducting part of the phase diagram, one may deduce a well-defined phase boundary in between.

Concerning the structural properties, we have observed that the tetragonal-to-orthorhombic phase transition extends to a rather large temperature regime with pronounced precursors persisting well above the long-range transition temperature. It is difficult to determine the transition temperature by diffraction techniques as long-range and short-range distortions are nearly impossible to separate. The analysis of the peak height of the nuclear Bragg peaks is certainly misleading. Similar precursor effects should also exist for the $RE\mathrm{O}_{1-x}\mathrm{F}_x\mathrm{FeAs}$ materials and might be one reason for discrepancies in the phase diagrams obtained by different groups. In $\mathrm{LaO}_{1-x}\mathrm{F}_x\mathrm{FeAs}$ the long-range orthorhombic distortion is fully suppressed by amounts of doping which are below the level needed to induce superconductivity. Taking further account of the magnetic neutron-diffraction results, we confirm the phase diagram presented in Ref. 19. However, we may not exclude that some orthorhombic precursors persist into the superconducting phase in $\mathrm{LaO}_{1-x}\mathrm{F}_x\mathrm{FeAs}$ as well as in other $RE\mathrm{O}_{1-x}\mathrm{F}_x\mathrm{FeAs}$ series.[10]

In pure and low-doped $\mathrm{LaO}_{1-x}\mathrm{F}_x\mathrm{FeAs}$, the onset of static magnetism as obtained by muon-spin relaxation[19] and by the temperature dependence of the magnetic Bragg peaks lies within the broad regime of the tetragonal-to-orthorhombic transition. For pure LaOFeAs, we find structural anomalies just above the onset of magnetism, as the FeAs distance and the FeAs layer thickness pass through a minimum in agreement with the effect observed for the thermal-expansion coefficient. These features seem to arise from the strong magnetoelastic coupling between the shape of the FeAs tetrahedra and the size of the magnetic moment suggesting that the enhancement of the antiferromagnetic correlations through the orthorhombic distortion implies a variation of the magnetic moment.

Note added in proof. After completion of the manuscript we learned that a single-crystal neutron-diffraction experiment on LaOFeAs finds a larger ordered moment consistent with the one we report here.[33]

ACKNOWLEDGMENTS

This work was supported by the Deutsche Forschungsgemeinschaft through the Sonderforschungsbereich 608, through the Forschergruppe 538 (Grant No. BU887/4), and through Grant No. BE1749/12. We thank M. Deutschmann, S. Müller-Litvanyi, S. Pichl, R. Müller, N. Leps, U. Stockert, and G. Friemel for support with sample synthesis and characterization. We further thank J. Rodríguez-Carvajal for the assistance with the powder-diffraction analysis.

*Corresponding author; qureshi@ph2.uni-koeln.de
†braden@ph2.uni-koeln.de

[1] Y. Kamihara, T. Watanabe, M. Hirano, and H. Hosono, J. Am. Chem. Soc. **130**, 3296 (2008).
[2] Z. A. Ren *et al.*, Chin. Phys. Lett. **25**, 2385 (2008).
[3] M. S. Torikachvili, S. L. Bud'ko, N. Ni, and P. C. Canfield, Phys. Rev. Lett. **101**, 057006 (2008).
[4] N. Ni, S. Nandi, A. Kreyssig, A. I. Goldman, E. D. Mun, S. L. Bud'ko, and P. C. Canfield, Phys. Rev. B **78**, 014523 (2008).
[5] T. Park, E. Park, H. Lee, T. Klimczuk, E. D. Bauer, F. Ronning, and J. D. Thompson, J. Phys.: Condens. Matter **20**, 322204 (2008).
[6] A. Kreyssig *et al.*, Phys. Rev. B **78**, 184517 (2008).
[7] P. Alireza, Y. T. C. Ko, C. M. P. J. Gillett, J. M. Cole, G. G. Lonzarich, and S. E. Sebastian, J. Phys.: Condens. Matter **21**, 012208 (2009).
[8] A. J. Drew *et al.*, Nature Mater. **8**, 310 (2009).
[9] S. A. J. Kimber *et al.*, Nature Mater. **8**, 471 (2009).
[10] J. Zhao *et al.*, Nature Mater. **7**, 953 (2008).
[11] C.-H. Lee, A. Iyo, H. Eisaki, H. Kito, M. T. F. Díaz, T. Ito, K. Kihou, H. Matsuhata, M. Braden, and K. Yamada, J. Phys. Soc. Jpn. **77**, 083704 (2008).
[12] Z. P. Yin, S. Lebègue, M. J. Han, B. P. Neal, S. Y. Savrasov, and W. E. Pickett, Phys. Rev. Lett. **101**, 047001 (2008).
[13] C. de la Cruz *et al.*, Nature (London) **453**, 899 (2008).
[14] T. Yildirim, Phys. Rev. Lett. **101**, 057010 (2008).
[15] M. A. McGuire *et al.*, Phys. Rev. B **78**, 094517 (2008).
[16] H. Maeter, H. Luetkens, Yu. G. Pashkevich, A. Kwadrin, R. Khasanov, A. Amato, A. A. Gusev, K. V. Lamonova, D. A. Chervinskii, R. Klingeler, C. Hess, G. Behr, B. Büchner, and H.-H. Klauss, Phys. Rev. B **80**, 094524 (2009).
[17] A. Kondrat *et al.*, Eur. Phys. J. B **70**, 461 (2009).
[18] X. Zhu, H. Yang, L. Fang, G. Mu, and H. H. Wen, Supercond. Sci. Technol. **21**, 105001 (2008).
[19] H. Luetkens *et al.*, Nature Mater. **8**, 305 (2009).
[20] L. Wang, U. Köhler, N. Leps, A. Kondrat, M. Nale, A. Gasparini, A. de Visser, G. Behr, C. Hess, R. Klingeler, and B. Büchner, Phys. Rev. B **80**, 094512 (2009).
[21] C. Hess, A. Kondrat, A. Narduzzo, J. E. Hamann-Borrero, R. Klingeler, J. Werner, G. Behr, and B. Büchner, EPL **87**, 17005 (2009).
[22] J. Dong, H. J. Zhang, G. Xu, Z. Li, G. Li, W. Z. Hu, D. Wu, G. F. Chen, X. Dai, J. L. Luo, Z. Fang, and N. L. Wang, EPL **83**, 27006 (2008).
[23] Q. Huang, J. Zhao, J. W. Lynn, G. F. Chen, J. L. Luo, N. L. Wang, and P. Dai, Phys. Rev. B **78**, 054529 (2008).
[24] J. Rodríguez-Carvajal, Physica B **192**, 55 (1993).
[25] R. Ballou and B. Ouladdiaf, in *Neutron Scattering from Magnetic Materials*, edited by T. Chatterji (Elsevier, New York, 2006).
[26] T. Inui, Y. Tanabe, and Y. Onodera, *Group Theory and Its Applications in Physics* (Springer-Verlag, Berlin, 1990).

[27] The propagation vector $\mathbf{k}=(0\ 1\ \frac{1}{2})$ is an equivalent option.
[28] J. Lynn and P. Dai, Physica C **469**, 469 (2009).
[29] A. C. Komarek, T. Taetz, M. T. Fernández-Díaz, D. M. Trots, A. Möller, and M. Braden, Phys. Rev. B **79**, 104425 (2009).
[30] J. -H. Chu, J. G. Analytis, K. De Greeve, P. L. McMahon, Z. Islam, Y. Yamamoto, and I. R. Fisher, Science **329**, 824 (2010).
[31] T. Nomura, S. W. Kim, Y. Kamihara, M. Hirano, P. V. Sushko, K. Kato, M. Takata, A. L. Shluger, and H. Hosono, Supercond. Sci. Technol. **21**, 125028 (2008).
[32] H.-J. Grafe, G. Lang, F. Hammerath, D. Paar, K. Manthey, K. Koch, H. Rosner, N. J. Curro, G. Behr, J. Werner, N. Leps, R. Klingeler, H.-H. Klauss, F. J. Litterst, and B. Büchner, New J. Phys. **11**, 035002 (2009).
[33] H.-F. Li, W. Tian, J.-Q. Yan, J. L. Zarestky, R. W. McCallum, T. A. Lograsso, and D. Vaknin, Phys. Rev. B **82**, 064409 (2010).